Localization and Criticality in Antiblockaded Two-Dimensional Rydberg Atom Arrays

Fangli Liu,[1] Zhi-Cheng Yang,[1] Przemyslaw Bienias,[1] Thomas Iadecola,[2] and Alexey V. Gorshkov[1]
[1]Joint Quantum Institute and Joint Center for Quantum Information and Computer Science, NIST/University of Maryland, College Park, Maryland 20742, USA
[2]Department of Physics and Astronomy, Iowa State University, Ames, Iowa 50011, USA

(Received 18 December 2020; revised 30 October 2021; accepted 13 December 2021; published 6 January 2022)

Controllable Rydberg atom arrays have provided new insights into fundamental properties of quantum matter both in and out of equilibrium. In this work, we study the effect of experimentally relevant positional disorder on Rydberg atoms trapped in a 2D square lattice under antiblockade (facilitation) conditions. We show that the facilitation conditions lead the connectivity graph of a particular subspace of the full Hilbert space to form a 2D Lieb lattice, which features a singular flat band. Remarkably, we find three distinct regimes as the disorder strength is varied: a critical regime, a delocalized but nonergodic regime, and a regime with a disorder-induced flat band. The critical regime's existence depends crucially upon the singular flat band in our model, and is absent in any 1D array or ladder system. We propose to use quench dynamics to probe the three different regimes experimentally.

DOI: 10.1103/PhysRevLett.128.013603

Recently, programmable Rydberg quantum simulators have attracted significant interest because they can provide insights into quantum matter's fundamental properties. With the rapid development of quantum technologies, synthetic arrays of Rydberg atoms with individual control are already available in one [1], two [2,3], and three dimensions [4]. Recent experiments on 1D Rydberg atom arrays have shed light on various phenomena, including nonequilibrium quantum many-body dynamics [5], the Kibble-Zurek mechanism [6], and quantum many-body scars [5,7]. The strong Rydberg-Rydberg interactions can also be used to realize quantum gates [8], making such systems promising platforms for quantum information processing [9,10].

Meanwhile, flat-band systems are conceptually important in condensed matter physics and can harbor both nontrivial topological properties [11–14] and strongly correlated phases arising from the enhanced interaction effects [15–22]. Recent work on twisted graphene heterostructures and circuit quantum electrodynamics (QED) opens up new venues for flat bands, enabling, respectively, the study of correlated insulators and superconductivity [23–26] and of quantum systems in hyperbolic space [27,28]. One particular direction of interest concerns the effect of disorder on flat-band eigenstates. It has been shown that such flat bands, when coupled to disorder, can lead to critical and multifractal phenomena absent in conventional Anderson localization [29–37].

In this work, we demonstrate that the physics of flat bands coupled to disorder can be naturally realized and probed using Rydberg atoms trapped in a 2D square lattice. We consider the so-called facilitation (antiblockade) mechanism, where the excitation of a Rydberg atom is strongly enhanced in the vicinity of an already excited atom [38–40]. Under such conditions, the full Hilbert space can effectively split into subspaces separated from one another by large energy scales. We focus on the manifold of states that can be created near-resonantly starting from a single Rydberg excitation. Within this subspace, the system can effectively be described by a single-particle hopping on a 2D Lieb lattice [40], which features a singular flat band in the clean limit. Although the Lieb lattice has been experimentally realized for photons [41–45], atoms [46,47], and electrons [48], the effect of disorder on flat-band states has not yet been systematically studied. We find that the interplay between positional disorder of Rydberg atom arrays and the synthetic flat-band states gives rise to a rich phase diagram, including a critical phase, a nonergodic extended phase, and a phase with a disorder-induced flat band. We show that these intriguing properties are essentially related to the singular flat band on the Lieb lattice and are absent in 1D and quasi-1D arrays.

Antiblockaded Rydberg atom array and mapping to Lieb lattice.—We consider the following Hamiltonian describing interacting Rydberg atoms trapped in a 2D $L \times L$ square lattice with spacing R_0:

$$H_{\mathrm{Ryd}} = \frac{\Omega}{2}\sum_{i=1}^{N}\sigma_i^x - \Delta\sum_{i=1}^{N} n_i + \frac{1}{2}\sum_{i\neq j=1}^{N} V(d_{ij}) n_i n_j, \quad (1)$$

where i and j run over sites of the square lattice [see Fig. 1(a)], $\sigma_i^x = |g_i\rangle\langle r_i| + |r_i\rangle\langle g_i|$, $|g_i\rangle$ ($|r_i\rangle$) denotes the ground (Rydberg) state of the ith atom, and $n_i = |r_i\rangle\langle r_i|$. The parameters Ω (Rabi frequency) and Δ (detuning) characterize coherent driving fields, while $V(d_{ij}) \propto 1/d_{ij}^6$

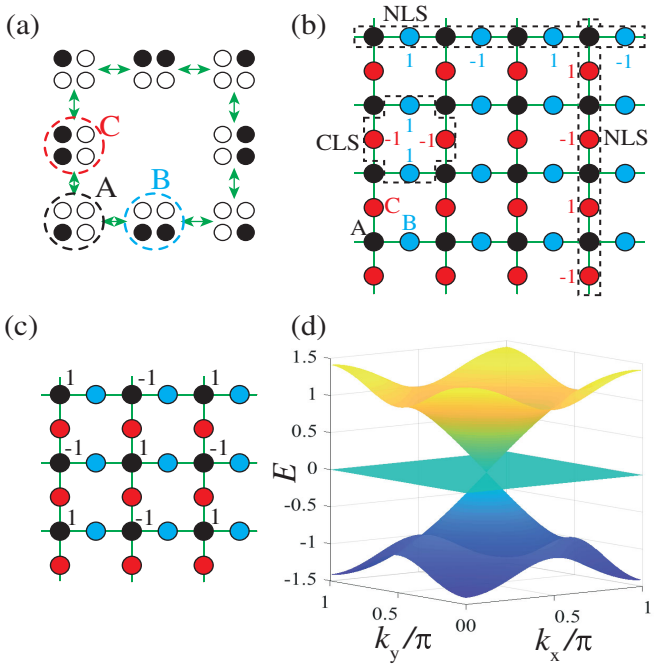

FIG. 1. (a) Under the antiblockade conditions, the connectivity graph of the subspace containing single isolated Rydberg excitations and single nearest-neighbor pairs thereof maps to a 2D Lieb lattice shown in (b). The black and white dots indicate atoms in Rydberg and ground states, respectively. Each unit cell of the Lieb lattice contains three sites: A, B, and C. (b) The flat-band eigenstates include compact localized states (CLSs), two noncontractible loop states (NLSs), and one noncompact state (NCS) shown in (c). The ± 1 indicate the relative wave function amplitudes for these states. (d) The band structure of the clean Lieb lattice, which contains two dispersive bands and one singular flat band.

quantifies the van der Waals interactions between atoms in Rydberg states at sites i and j (separated by distance d_{ij}). The antiblockade (facilitation) condition is obtained by setting $\Delta = V(R_0)$, so that an isolated excitation makes the excitation of its nearest-neighbor resonant [38–40]. We work in the limit $|\Delta| \gg \Omega$ where the unfacilitated excitations are sufficiently off resonant. We additionally require $V(\sqrt{2}R_0), V(2R_0) \gg \Omega$, so that a pair of neighboring Rydberg excitations is unable to further facilitate the excitation of any neighboring site. Hereafter we take $V(R_0) = 300\Omega$.

Under these conditions, the Hilbert space effectively splits into subspaces that are separated by energy scales much larger than Ω [39]. Here we focus on the simplest nontrivial subspace, whose degrees of freedom are hardcore bosons consisting of either a single Rydberg excitation or a pair of neighboring Rydberg excitations. One can readily see that the connectivity graph of states in this subspace forms a 2D Lieb lattice [see Figs. 1(a)–1(b)]. The Hamiltonian (1) thus reduces to a single-particle hopping on this lattice. The Lieb lattice contains three sites per unit cell, where the A site corresponds to a single Rydberg excitation in the original model, while the B and C sites correspond, respectively, to horizontal and vertical pairs of neighboring Rydberg excitations [see Supplemental Material (SM) for more details [49]].

Flat band on the Lieb lattice.—The single-particle hopping Hamiltonian on the Lieb lattice takes the form

$$H_{\mathrm{Lieb}} = \sum_{\langle i,j \rangle} \Omega c_i^\dagger c_j + \mathrm{H.c.}, \tag{2}$$

where $\langle i, j \rangle$ denotes nearest-neighbor sites on the Lieb lattice, as shown in Fig. 1(b). The energy spectrum of Hamiltonian (2) contains two dispersive bands $E_\pm(\boldsymbol{k}) = \pm\Omega\sqrt{\cos^2(k_x) + \cos^2(k_y)}$ and one flat band $E = 0$ [see Fig. 1(d)]. The zero-energy flat band touches the two dispersive bands at $k_x = k_y = \pi/2$, leading to a threefold degeneracy at this point. As shown in Refs. [50,51], the band touching in this model is in fact irremovable, which signals a singularity in the Bloch wave function. The $E = 0$ band of Hamiltonian (2) in this case is known as a *singular* flat band. The singularity of the flat band has important consequences on the eigenstates within the band. Generically, the eigenstates of a flat band are localized in real space; hence, the name compact localized states (CLSs) [see Fig. 1(b) for the Lieb lattice]. When the flat band is nonsingular, such CLSs form a complete basis of the flat band. By contrast, when the flat band is singular, the set of all CLSs is not linearly independent. For the Lieb lattice, there exist three additional extended eigenstates of the flat band: two noncontractible loop states (NLSs) [Fig. 1(b)] and one noncompact state (NCS) [Fig. 1(c)].

Positional disorder.—Small deviations of atomic positions from the centers of the corresponding traps can significantly affect the atom-atom interaction. The thermal distribution of atomic positions can be described as a Gaussian with width σ (measured in units of R_0) [10,39]. Ignoring atomic motion during the experiment (frozen-gas approximation) [39], such randomness enters Eq. (1) via the interaction term: $V(R) = V(R_0 + \delta R) \approx V(R_0) + \delta V$, where δV is a random time-independent shift potential caused by the displacement. This position-disordered interaction manifests itself on the effective Lieb lattice as random, but correlated, on-site potentials for the B and C sublattices. Since the position disorder only affects Rydberg-Rydberg interactions, the A sublattice sites, which represent single Rydberg excitations, do not couple to disorder. Therefore, while the CLSs and NLSs are supported on B and C sublattices and hence are no longer exact eigenstates of the disordered Hamiltonian, the noncompact state in Fig. 1(c) remains unaffected by disorder.

To study the effect of disorder on the singular flat band, we numerically diagonalize the Lieb lattice Hamiltonian (2) in real space with positional disorder on an $L \times L$ square lattice. We focus on the middle one third of eigenstates in

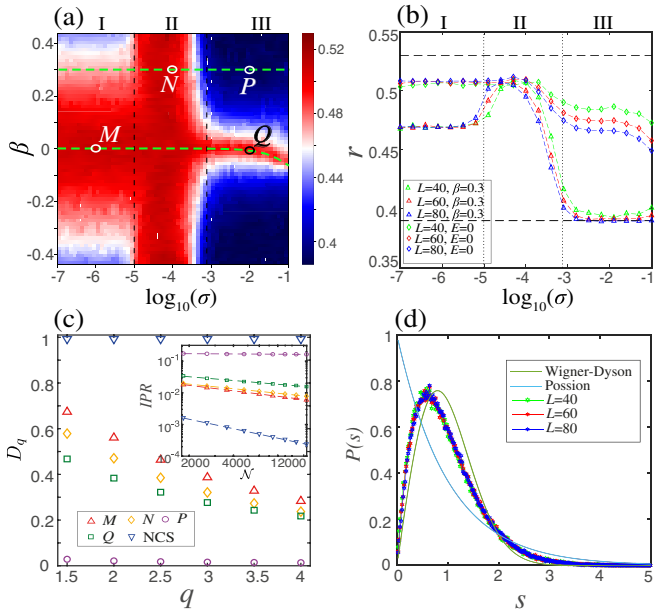

FIG. 2. (a) Level-spacing ratio r versus the rescaled eigenstate label β and disorder strength σ. (b) r as a function of disorder strength for two cuts, shown by dashed lines in (a), along $E = 0$ and $\beta = 0.3$ for different system sizes. The error bars (not shown) are smaller than the plot markers. (c) Fractal dimension D_q versus q, for states at representative points in (a): M $(\beta = 0, \log_{10}\sigma = -6)$, N $(\beta = 0.3, \log_{10}\sigma = -4)$, P $(\beta = 0, \log_{10}\sigma = -2)$, Q $(\beta = 0.3, \log_{10}\sigma = -2)$, as well as the noncompact zero-energy eigenstate (NCS) for arbitrary disorder strength. Inset: Scaling of IPR as a function of the Hilbert-space dimension. (d) Probability distribution of the unfolded level spacings $P(s)$ for states in regime I for different system sizes [52].

the spectrum, which corresponds to the flat-band states in the clean limit. We rank order the eigenstates according to their energies $E_i > E_{i-1}$ and introduce a rescaled label $\beta = [(i - \mathcal{N}/2)/(\mathcal{N}/3)] \in (-0.5, 0.5)$, where $\mathcal{N}$ is the Hilbert-space dimension and $i \in (\mathcal{N}/3, 2\mathcal{N}/3)$. We probe ergodicity versus localization using the level-spacing ratio $r_i = \min(\delta_i, \delta_{i+1})/\max(\delta_i, \delta_{i+1})$, where $\delta_i = E_{i+1} - E_i$. Ergodic and localized phases are characterized by a Wigner-Dyson (WD) distributed spectrum with mean $\bar{r} \approx 0.53$ and a Poisson distributed spectrum with $\bar{r} \approx 0.39$, respectively. Figure 2(a) shows the eigenstate-resolved r as the disorder strength σ varies. We find a rich phase diagram featuring three distinct regimes: a critical regime I, a nonergodic extended regime II, and a regime III, in which a disorder-induced flat band emerges (see Table I for the main features). Below, we discuss each regime in detail.

Regime I: Criticality.—Let us first focus on the weak-disorder regime, where the level-spacing statistics are intermediate between WD and Poisson, with the band-edge states [near the top and bottom of Fig. 2(a)] being more localized. As one can see from Fig. 3(a), while the wave function is extended in real space, it appears less ergodic than a perfectly delocalized state. Moreover, the wave function is mainly supported on the B and C sublattices [inset of Fig. 3(a)] [49], indicating that the flat-band states do not couple strongly to the original dispersing bands at weak disorder. To characterize the wave functions more quantitatively, we study the inverse participation ratio (IPR) $I_q(\beta) = \langle \sum_i |\psi_i^\alpha|^{2q} \rangle$, where ψ_i^α is the amplitude of the αth wave function on site i and the average is taken over disorder realizations and over a fixed number of states α around β [53]. It is in general expected to scale as $I_q \sim \mathcal{N}^{-D_q(q-1)}$, where D_q is known as the fractal dimension, with $D_q = 1$ for ergodic states and $D_q = 0$ for localized states. If D_q depends on q, as occurs, for example, at the critical point of the Anderson transition [53–57], the eigenstates are called multifractal. Figure 2(c) shows the exponent D_q extracted from the IPR for point M in Fig. 2(a), which indeed exhibits a q dependence, signaling multifractality and nonergodicity of the wave functions in this regime [58,59].

Besides delocalization and nonergodicity of the wave functions, another interesting feature in regime I is that the level-spacing statistics is intermediate between WD and Poisson and shows almost no dependence on system size [Fig. 2(b)]. This is also clear from Fig. 2(d), where we plot the distribution $P(s)$ of the level spacing s, after spectral unfolding [29,60], for the states shown in Fig. 2(a), i.e., the middle one third of the states. This suggests that the level statistics remain intermediate between WD and Poisson in the thermodynamic limit; such statistics are called critical [29,36,59,61–63]. The statistics also show little dependence on disorder strength, suggesting that the entire regime I is critical even for extremely weak disorder [29,36]. This is in contrast to the standard Anderson [53] and many-body [55] localization transitions, which involve a single critical point. The origin of the criticality in regime I lies in the singular nature of the flat band in Hamiltonian (2). As shown in Ref. [29], for a flat band with a singular band touching, the real-space matrix elements of the projection operator onto the flat band $\langle \mathbf{R}|\mathcal{P}|\mathbf{R} + \mathbf{r}\rangle$ decay as $|\mathbf{r}|^{-d}$ in d

TABLE I. Main features of three distinct localization regimes.

	Wave function	Support	Feature
Regime I	Critical, multifractal	B, C	Original flat band
Regime II	Multifractal	A, B, C	Hybridization with dispersive bands
Regime III	Localized ($\lvert E\rvert \gtrsim 0$), multifractal ($E \approx 0$)	A	Disorder-induced flat band

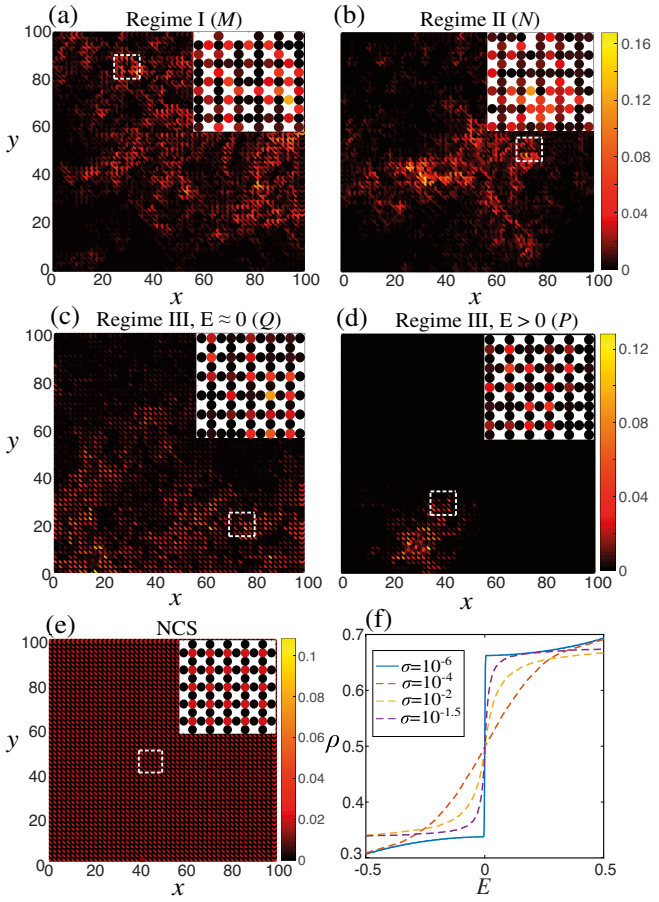

FIG. 3. (a)–(d) Amplitudes of the real-space wave functions for representative points M (a), N (b), Q (c), and P (d) in Fig. 2(a). (e) The amplitudes of the wave function for the noncompact eigenstate. Each inset shows an enlarged view locally. (f) The integrated density of states as a function of energy, for different disorder strengths.

dimensions. States originating from such flat bands are generically critical in the presence of weak disorder. On the other hand, for nonsingular flat bands (e.g., in 1D ladder systems), $\langle \mathbf{R}|\mathcal{P}|\mathbf{R}+\mathbf{r}\rangle$ decays exponentially with $\mathbf{r}$ and one can use the detangling method [39,40,47] to observe conventional Anderson localization.

Regime II: Hybridization with dispersive bands.—Similarly to regime I, the level-spacing statistics in regime II are also intermediate between WD and Poisson, as shown in Fig. 2(a). However, the physics in these two regimes is drastically different. To see this, let us first look at a representative real-space eigenstate in regime II, shown in Fig. 3(b) [49]. Although the wave function is again extended but nonergodic, it now has support on all three sublattices [inset of Fig. 3(b)], indicating that the original flat band strongly hybridizes with the dispersive bands as the disorder strength increases. Moreover, the fractal dimension D_q again exhibits a q dependence, indicating multifractality in this regime. Nonetheless, regime II no longer appears critical, as can be seen from the noticeable but subtle system size dependence of the level statistics in Fig. 2(b) [49].

Regime III: Disorder-induced flat band.—In the strongly disordered regime, one expects that most of the eigenstates become localized, as is indeed confirmed by the level-spacing statistics in Fig. 2(a). The real-space wave function shown in Fig. 3(d) and the fractal dimension $D_q \approx 0$ in Fig. 2(c) are also consistent with the states being localized. However, we find that in the middle of the spectrum where the energies are very close to $E = 0$, the eigenstates are *delocalized* [see Fig. 3(c)]. The fractal dimension of these delocalized states exhibits a q dependence [see Fig. 2(c)], indicating multifractality. Moreover, the integrated density of states in Fig. 3(f) shows a sharper jump near $E = 0$ compared to the more weakly disordered regime II and, counterintuitively, becomes sharper with increasing disorder. This indicates the presence of a flat band in the strong-disorder regime. This disorder-induced flat band is physically distinct from the original flat band of Hamiltonian (2) in the clean limit [solid curve in Fig. 3(f)]. As can be seen from Figs. 3(c) and 3(d), the flat-band states in the strong-disorder regime have dominant support on sublattice A [49], whereas the original flat-band states are supported on sublattices B and C instead [see Fig. 3(a)].

To understand this disorder-induced flat band, we can write down the eigenvalue equation for the single-particle hopping Hamiltonian in real space (see SM [49] for the details of the analysis in this paragraph). By eliminating sublattice A [64], one arrives at a single-particle hopping model on the B and C sublattices only, which form a *planar pyrochlore lattice*. As shown in Refs. [29,51], the planar pyrochlore lattice also hosts a singular flat band at $E = 0$ in the clean limit, and the flat band eigenstates become multifractal states with $E \approx 0$ in the presence of weak disorder [see also Fig. 2(a)]. That the wave functions have dominant support on sublattice A in regime III (and dominate support on B and C sublattices in regime I) can also be understood using the elimination procedure.

We stress that the disorder-induced flat band in regime III only arises in the Rydberg atom setup, where disorder naturally couples to sublattices B and C only. In contrast, when disorder is present on all sublattices, as is usually the case, the density of states will instead have a broad distribution and no flat band is formed [49].

Quench dynamics.—The three regimes discussed above have distinct dynamical features in quantum quench experiments (see SM [49] for numerical results). We choose three different types of initial states, including a CLS, a state with nearest-neighbor Rydberg excitations, and a state with a single excitation, all of which can be prepared in experiments [40]. The Rydberg excitation probabilities have initial-state-dependent distinct features under time evolution by the 2D disordered Lieb-lattice Hamiltonian in the three respective regimes.

Conclusions and outlook.—We have studied the effect of disorder on 2D Rydberg atom arrays in the antiblockade regime and uncovered rich localization phenomena depending on the disorder strength. In contrast to previous works [29–37], our study originates from an interacting Rydberg system, and our predictions hold even in the full quantum many-body system (see SM [49]). Besides the Rydberg system, our results are also relevant to general disorder types [49] in other Lieb-lattice implementations, e.g., optical [41–45] and microwave [27] photons, cold atoms [46,47], and electrons [48,65]. By changing the antiblockade conditions, our study can be extended to a wide variety of synthetic graphs. Moreover, our construction generically leads to single-particle hopping models on effective graphs that are subdivisions of the graph corresponding to the physical lattice. We expect the nonergodic extended states uncovered in this work and disorder-induced flat bands to be generic for graphs with singular flat bands under this construction. Another interesting direction is to consider 3D generalizations of our study involving the interplay of conventional Anderson localization with a mobility edge and the degenerate singular bands. Finally, it would be interesting to consider subspaces with multiple excitations, where there can be nontrivial interplay of antiblockade conditions and many-body interactions [66–68] (or blockade constraints) in the synthetic lattice.

We thank Igor Boettcher, Adam Ehrenberg, Luis Pedro García-Pintos, Alicia Kollár, Rex Lundgren, and Oles Shtanko for helpful discussions. F. L., Z.-C. Y., P. B., and A. V. G. acknowledge funding by AFOSR, NSF (QLCI Grant No. OMA-2120757), U.S. Department of Energy Award No. DE-SC0019449, AFOSR MURI, the DOE ASCR Quantum Testbed Pathfinder program (Award No. DE-SC0019040), DOE ASCR Accelerated Research in Quantum Computing program (Award No. DE-SC0020312), NSF PFCQC program, ARO MURI, ARL CDQI, and NSF PFC at JQI. Z.-C. Y. is also supported by MURI ONR N00014-20-1-2325, MURI AFOSR, FA9550-19-1-0399, and Simons Foundation. T. I. acknowledges Iowa State University startup funds.

[1] M. Endres, H. Bernien, A. Keesling, H. Levine, E. R. Anschuetz, A. Krajenbrink, C. Senko, V. Vuletic, M. Greiner, and M. D. Lukin, Atom-by-atom assembly of defect-free one-dimensional cold atom arrays, Science **354**, 1024 (2016).

[2] D. Barredo, S. D. Léséleuc, V. Lienhard, T. Lahaye, and A. Browaeys, An atom-by-atom assembler of defect-free arbitrary two-dimensional atomic arrays, Science **354**, 1021 (2016).

[3] E. Guardado-Sanchez, P. T. Brown, D. Mitra, T. Devakul, D. A. Huse, P. Schauß, and W. S. Bakr, Probing the Quench Dynamics of Antiferromagnetic Correlations in a 2D Quantum Ising Spin System, Phys. Rev. X **8**, 021069 (2018).

[4] D. Barredo, V. Lienhard, S. de Léséleuc, T. Lahaye, and A. Browaeys, Synthetic three-dimensional atomic structures assembled atom by atom, Nature (London) **561**, 79 (2018).

[5] H. Bernien, S. Schwartz, A. Keesling, H. Levine, A. Omran, H. Pichler, S. Choi, A. S. Zibrov, M. Endres, M. Greiner, V. Vuletić, and M. D. Lukin, Probing many-body dynamics on a 51-atom quantum simulator, Nature (London) **551**, 579 (2017).

[6] A. Keesling, A. Omran, H. Levine, H. Bernien, H. Pichler, S. Choi, R. Samajdar, S. Schartz, P. Silvi, S. Sachdev, P. Zoller, M. Endres, M. Greiner, V. Vuletić, and M. D. Lukin, Quantum Kibble-Zurek mechanism and critical dynamics on a programmable Rydberg simulator, Nature (London) **568**, 207 (2019).

[7] C. J. Turner, A. A. Michailidis, D. A. Abanin, M. Serbyn, and Z. Papić, Weak ergodicity breaking from quantum many-body scars, Nat. Phys. **14**, 745 (2018).

[8] H. Levine, A. Keesling, G. Semeghini, A. Omran, T. T. Wang, S. Ebadi, H. Bernien, M. Greiner, V. Vuletić, H. Pichler, and M. D. Lukin, Parallel Implementation of High-Fidelity Multiqubit Gates with Neutral Atoms, Phys. Rev. Lett. **123**, 170503 (2019).

[9] H. Levine, A. Keesling, A. Omran, H. Bernien, S. Schwartz, A. S. Zibrov, M. Endres, M. Greiner, V. Vuletić, and M. D. Lukin, High-Fidelity Control and Entanglement of Rydberg-Atom Qubits, Phys. Rev. Lett. **121**, 123603 (2018).

[10] A. Omran, H. Levine, A. Keesling, G. Semeghini, T. T. Wang, S. Ebadi, H. Bernien, A. S. Zibrov, H. Pichler, S. Choi, J. Cui, M. Rossignolo, P. Rembold, S. Montangero, T. Calarco, M. Endres, M. Greiner, V. Vuletić, and M. D. Lukin, Generation and manipulation of Schrödinger cat states in Rydberg atom arrays, Science **365**, 570 (2019).

[11] K. Sun, Z. Gu, H. Katsura, and S. Das Sarma, Nearly Flatbands with Nontrivial Topology, Phys. Rev. Lett. **106**, 236803 (2011).

[12] E. Tang, J.-W. Mei, and X.-G. Wen, High-Temperature Fractional Quantum Hall States, Phys. Rev. Lett. **106**, 236802 (2011).

[13] T. Neupert, L. Santos, C. Chamon, and C. Mudry, Fractional Quantum Hall States at Zero Magnetic Field, Phys. Rev. Lett. **106**, 236804 (2011).

[14] N. Y. Yao, C. R. Laumann, A. V. Gorshkov, S. D. Bennett, E. Demler, P. Zoller, and M. D. Lukin, Topological Flat Bands from Dipolar Spin Systems, Phys. Rev. Lett. **109**, 266804 (2012).

[15] E. H. Lieb, Two Theorems on the Hubbard Model, Phys. Rev. Lett. **62**, 1201 (1989).

[16] A. Mielke, Ferromagnetism in the Hubbard model on line graphs and further considerations, J. Phys. A **24**, 3311 (1991).

[17] D. Leykam, A. Andreanov, and S. Flach, Artificial flat band systems: from lattice models to experiments, Adv. Phys. **3**, 1473052 (2018).

[18] N. Regnault and B. A. Bernevig, Fractional Chern Insulator, Phys. Rev. X **1**, 021014 (2011).

[19] E. J. Bergholtz and Z. Liu, Topological flat band models and fractional Chern insulators, Int. J. Mod. Phys. B **27**, 1330017 (2013).

[20] Z. Liu, E. J. Bergholtz, H. Fan, and A. M. Läuchli, Fractional Chern Insulators in Topological Flat Bands with Higher Chern Number, Phys. Rev. Lett. **109**, 186805 (2012).
[21] N. Y. Yao, A. V. Gorshkov, C. R. Laumann, A. M. Läuchli, J. Ye, and M. D. Lukin, Realizing Fractional Chern Insulators in Dipolar Spin Systems, Phys. Rev. Lett. **110**, 185302 (2013).
[22] G. Zhu, J. Koch, and I. Martin, Nematic quantum liquid crystals of bosons in frustrated lattices, Phys. Rev. B **93**, 144508 (2016).
[23] Y. Cao, V. Fatemi, A. Demir, S. Fang, S. L. Tomarken, J. Y. Luo, J. D. Sanchez-Yamagishi, K. Watanabe, T. Taniguchi, E. Kaxiras, R. C. Ashoori, and P. Jarillo-Herrero, Correlated insulator behaviour at half-filling in magic-angle graphene superlattices, Nature (London) **556**, 80 (2018).
[24] Y. Cao, V. Fatemi, S. Fang, K. Watanabe, T. Taniguchi, E. Kaxiras, and P. Jarillo-Herrero, Unconventional superconductivity in magic-angle graphene superlattices, Nature (London) **556**, 43 (2018).
[25] M. Yankowitz, S. Chen, H. Polshyn, Y. Zhang, K. Watanabe, T. Taniguchi, D. Graf, A. F Young, and C. R Dean, Tuning superconductivity in twisted bilayer graphene, Science **363**, 1059 (2019).
[26] H. C. Po, L. Zou, A. Vishwanath, and T. Senthil, Origin of Mott Insulating Behavior and Superconductivity in Twisted Bilayer Graphene, Phys. Rev. X **8**, 031089 (2018).
[27] A. J. Kollar, M. Fitzpatrick, and A. A. Houck, Hyperbolic lattices in circuit quantum electrodynamics, Nature (London) **571**, 45 (2019).
[28] A. J. Kollár, M. Fitzpatrick, P. Sarnak, and A. A. Houck, Line-graph lattices: Euclidean and non-euclidean flat bands, and implementations in circuit quantum electrodynamics, Commun. Math. Phys. **376**, 1919 (2020).
[29] J. T. Chalker, T. S. Pickles, and P. Shukla, Anderson localization in tight-binding models with flat bands, Phys. Rev. B **82**, 104209 (2010).
[30] D. Leykam, S. Flach, O. Bahat-Treidel, and A. S. Desyatnikov, Flat band states: Disorder and nonlinearity, Phys. Rev. B **88**, 224203 (2013).
[31] M. Goda, S. Nishino, and H. Matsuda, Inverse Anderson Transition Caused by Flatbands, Phys. Rev. Lett. **96**, 126401 (2006).
[32] J. H. Wilson, Y. Fu, S. Das Sarma, and J. H. Pixley, Disorder in twisted bilayer graphene, Phys. Rev. Research **2**, 023325 (2020).
[33] J. H. Wilson, D. A. Huse, S. Das Sarma, and J. H. Pixley, Avoided quantum criticality in exact numerical simulations of a single disordered Weyl cone, Phys. Rev. B **102**, 100201 (R) (2020).
[34] Y. Fu, J. H. Wilson, and J. H. Pixley, Flat topological bands and eigenstate criticality in a quasiperiodic insulator, arXiv:2003.00027.
[35] S. D. Huber and E. Altman, Bose condensation in flat bands, Phys. Rev. B **82**, 184502 (2010).
[36] P. Shukla, Disorder perturbed flat bands. II. Search for criticality, Phys. Rev. B **98**, 184202 (2018).
[37] C. Gneiting, Z. Li, and F. Nori, Lifetime of flatband states, Phys. Rev. B **98**, 134203 (2018).
[38] M. Mattioli, A. W. Glätzle, and W. Lechner, From classical to quantum non-equilibrium dynamics of Rydberg excitations in optical lattices, New J. Phys. **17**, 113039 (2015).
[39] M. Marcuzzi, J. Minář, D. Barredo, S. de Léséleuc, H. Labuhn, T. Lahaye, A. Browaeys, E. Levi, and I. Lesanovsky, Facilitation Dynamics and Localization Phenomena in Rydberg Lattice Gases with Position Disorder, Phys. Rev. Lett. **118**, 063606 (2017).
[40] M. Ostmann, M. Marcuzzi, J. Minář, and I. Lesanovsky, Synthetic lattices, flat bands and localization in Rydberg quantum simulators, Quantum Sci. Technol. **4**, 02LT01 (2019).
[41] S. Mukherjee, A. Spracklen, D. Choudhury, N. Goldman, P. Öhberg, E. Andersson, and R. R. Thomson, Observation of a Localized Flat-Band State in a Photonic Lieb Lattice, Phys. Rev. Lett. **114**, 245504 (2015).
[42] R. A. Vicencio, C. Cantillano, L. Morales-Inostroza, B. Real, C. Mejía-Cortés, S. Weimann, A. Szameit, and M. I. Molina, Observation of Localized States in Lieb Photonic Lattices, Phys. Rev. Lett. **114**, 245503 (2015).
[43] F. Diebel, D. Leykam, S. Kroesen, C. Denz, and A. S. Desyatnikov, Conical Diffraction and Composite Lieb Bosons in Photonic Lattices, Phys. Rev. Lett. **116**, 183902 (2016).
[44] D. Guzmán-Silva, C. Mejía-Cortés, M. A. Bandres, M. C. Rechtsman, S. Weimann, S. Nolte, M. Segev, A. Szameit, and R. A. Vicencio, Experimental observation of bulk and edge transport in photonic Lieb lattices, New J. Phys. **16**, 063061 (2014).
[45] S. Xia, Y. Hu, D. Song, Y. Zong, L. Tang, and Z. Chen, Demonstration of flat-band image transmission in optically induced Lieb photonic lattices, Opt. Lett. **41**, 1435 (2016).
[46] S. Taie, H. Ozawa, T. Ichinose, T. Nishio, S. Nakajima, and Y. Takahashi, Coherent driving and freezing of bosonic matter wave in an optical Lieb lattice, Sci. Adv. **1**, e1500854 (2015).
[47] F. Baboux, L. Ge, T. Jacqmin, M. Biondi, E. Galopin, A. Lemaître, L. Le Gratiet, I. Sagnes, S. Schmidt, H. E. Türeci, A. Amo, and J. Bloch, Bosonic Condensation and Disorder-Induced Localization in a Flat Band, Phys. Rev. Lett. **116**, 066402 (2016).
[48] M. R. Slot, T. S. Gardenier, P. H. Jacobse, G. C. P. v. Miert, S. N. Kempkes, S. J. M. Zevenhuizen, C. M. Smith, D. Vanmaekelbergh, and I. Swart, Experimental realization and characterization of an electronic Lieb lattice, Nat. Phys. **13**, 672 (2017).
[49] See Supplemental Material at http://link.aps.org/supplemental/10.1103/PhysRevLett.128.013603 for mapping from the original lattice to the Lieb lattice, derivation of the effective planar-pyrochlore hopping model, level spacing statistics in regime II, sublattice-resolved wave function weight distributions in each regime, additional numerical results on uncorrelated disorders as well as disorders that couple to all sublattices, numerical results for the quench dynamics in three regimes, and numerical results for the full quantum many-body system.
[50] D. L. Bergman, C. Wu, and L. Balents, Band touching from real-space topology in frustrated hopping models, Phys. Rev. B **78**, 125104 (2008).

[51] J.-W. Rhim and B.-J. Yang, Classification of flat bands according to the band-crossing singularity of Bloch wave functions, Phys. Rev. B **99**, 045107 (2019).
[52] In Figs. 2(a)–2(c), each point represents an average over eigenstates in an energy window containing $1/24$ of the total number of eigenstates. All data shown in Figs. 2(a)–(d) are averaged over 800 realizations of disorder.
[53] F. Evers and A. D. Mirlin, Anderson transitions, Rev. Mod. Phys. **80**, 1355 (2008).
[54] D. J. Luitz, F. Alet, and N. Laflorencie, Universal Behavior beyond Multifractality in Quantum Many-Body Systems, Phys. Rev. Lett. **112**, 057203 (2014).
[55] N. Macé, F. Alet, and N. Laflorencie, Multifractal Scalings Across the Many-Body Localization Transition, Phys. Rev. Lett. **123**, 180601 (2019).
[56] J. Lindinger, A. Buchleitner, and A. Rodríguez, Many-Body Multifractality throughout Bosonic Superfluid and Mott Insulator Phases, Phys. Rev. Lett. **122**, 106603 (2019).
[57] R. Menu and T. Roscilde, Anomalous Diffusion and Localization in a Positionally Disordered Quantum Spin Array, Phys. Rev. Lett. **124**, 130604 (2020).
[58] B. L. Altshuler, E. Cuevas, L. B. Ioffe, and V. E. Kravtsov, Nonergodic Phases in Strongly Disordered Random Regular Graphs, Phys. Rev. Lett. **117**, 156601 (2016).
[59] A. De Luca, B. L. Altshuler, V. E. Kravtsov, and A. Scardicchio, Anderson Localization on the Bethe Lattice: Nonergodicity of Extended States, Phys. Rev. Lett. **113**, 046806 (2014).
[60] S. Nishino, H. Matsuda, and M. Goda, Flat-band localization in weakly disordered system, J. Phys. Soc. Jpn. **76**, 024709 (2007).
[61] B. I. Shklovskii, B. Shapiro, B. R. Sears, P. Lambrianides, and H. B. Shore, Statistics of spectra of disordered systems near the metal-insulator transition, Phys. Rev. B **47**, 11487 (1993).
[62] Y. Huang and B. I. Shklovskii, Anderson transition in three-dimensional systems with non-hermitian disorder, Phys. Rev. B **101**, 014204 (2020).
[63] X. Deng, B. L. Altshuler, G. V. Shlyapnikov, and L. Santos, Quantum Levy Flights and Multifractality of Dipolar Excitations in a Random System, Phys. Rev. Lett. **117**, 020401 (2016).
[64] M. Hilke, Localization properties of the periodic random Anderson model, J. Phys. A **30**, L367 (1997).
[65] W. Jiang, H. Huang, and F. Liu, A Lieb-like lattice in a covalent-organic framework and its Stoner ferromagnetism, Nat. Commun. **10**, 2207 (2019).
[66] Y. Kuno, T. Orito, and I. Ichinose, Flat-band many-body localization and ergodicity breaking in the creutz ladder, New J. Phys. **22**, 013032 (2020).
[67] C. Danieli, A. Andreanov, and S. Flach, Many-body flatband localization, Phys. Rev. B **102**, 041116(R) (2020).
[68] N. Roy, A. Ramachandran, and A. Sharma, Compact, flat-band based, Anderson and many-body localization in a diamond chain, arXiv:1912.09951.